# Effects of crust and mantle heterogeneity on PP/P and SS/S amplitude ratios

Jeroen Ritsema,[1] Luis A. Rivera,[2] Dimitri Komatitsch,[1] Jeroen Tromp,[1] and Hendrik-Jan van Heijst[1, 3]

[1] Long-period (T > 16 s) PP/P and SS/S amplitude ratios have coherent geographic variations. On average, PP/P is ∼10% higher than predicted by the Preliminary Reference Earth Model (PREM) when PP surface-reflection points are within continental regions, and ∼10% lower than PREM predictions for oceanic reflection points. Spectral-element synthetics show that this variation can be attributed mostly to the effect of crustal thickness on the long-period PP reflection coefficient. The anomalies of SS/S are similar in amplitude but their geographic variation does not obviously correlate with ocean/continent variations. The variation of SS/S determined from spectral-element waveforms of S and SS for 3-D models of the crust and mantle is similar to the observed variation of SS/S. This suggests that wave propagation effects are largely responsible for the observed SS/S variation, not only intrinsic attenuation. *INDEX TERMS:* 7203 Seismology: Body wave propagation; 7205 Seismology: Continental crust (1242); 7260 Seismology: Theory and modeling; 5144 Physical Properties of Rocks: Wave attenuation

## 1. Introduction

[2] The high level of correlation between global models of shear-velocity heterogeneity indicates that, at least at long wavelengths, the shear-velocity structure of the mantle is well known [e.g., *Dziewonicz*, 2000]. Tomographic models to date are constrained primarily by body-wave travel-time and surface-wave phase-delay measurements. Seismic wave amplitudes can provide complementary constraints on velocity heterogeneity as well as attenuation. However, modeling of amplitudes is difficult. Surface-wave amplitude measurements display a large scatter. Hence, models based on these data are necessarily low in spatial resolution compared to travel-time and phase-velocity models [*Woodhouse and Wong*, 1986; *Romanowicz*, 1990, 1995; *Selby and Woodhouse*, 2000; *Billien et al.*, 2000].

[3] In this paper, we analyze a global data set of PP/P and SS/S amplitude ratios following recent analyses of the body-wave phases S and SS by *Bhattacharyya et al.* [1996] and *Reid et al.* [2001]. Contrary to amplitudes of individual body-wave phases, the precision of PP/P and SS/S amplitude ratios is not compromised by uncertainties in earthquake source parameters (e.g., epicenter, mechanism, and seismic moment). Using the spectral-element method (SEM) developed by *Komatitsch and Tromp* [2002a, 2002b], we demonstrate that the effects of seismic wave focusing and defocusing cause long-period body-wave amplitude

variations in addition to surface-wave amplitude variations with patterns similar to those seen in the data.

## 2. Measurement of Amplitude Ratios

### 2.1. Observations

[4] Using broadband waveform data from the GSN and GEOSCOPE networks (1980–2000), we measure PP/P and SS/S amplitude ratios with respect to the Preliminary Reference Earth Model (PREM) [*Dziewonski and Anderson*, 1981]. We make these measurements by cross-correlating low-pass filtered (T > 16 s) observed and synthetic waveforms. The synthetics are computed by normal-mode summation using the PREM velocity and Q structure and Harvard CMT source parameters.

[5] We define the correlation function between the observed, $d(t)$, and synthetic, $s(t)$, waveforms within a window $W$ by:

$$\Psi_{ds}(\tau) = \int_W d(t)s(t-\tau)\mathrm{d}t. \tag{1}$$

First, we determine the time shift $\tau_m$ of the synthetic waveform for which $\Psi_{ds}(\tau)$ has its maximum value. This time shift is regarded as the body-wave travel-time delay. Given $\tau_m$, we define two quantities that characterize the amplitude ratio between $d(t)$ and $s(t-\tau_m)$:

$$A_1 = \frac{\Psi_{ds}(\tau_m)}{\Psi_{ss}(\tau_m)}$$

and

$$A_2 = \frac{\Psi_{dd}(\tau_m)}{\Psi_{ds}(\tau_m)}. \tag{2}$$

$A_1$ and $A_2$ minimize, respectively,

$$\int_W [d(t) - A_1 s(t-\tau_m)]^2 \mathrm{d}t$$

and

$$\int_W \left[A_2^{-1} d(t) - s(t-\tau_m)\right]^2 \mathrm{d}t. \tag{3}$$

Using vertical component recordings, we measure $A_1^P$, $A_2^P$, $A_1^{PP}$, and $A_2^{PP}$ for 80-s wide time windows centered on the theoretical arrival times of P and PP, respectively. $A_1$ is equal to $A_2$ only when the waveforms of $d(t)$ and $s(t)$ in the cross-correlation window $W$ are identical. Therefore we obtain

$$A_1^{\mathrm{PP/P}} = \frac{\min\left(A_1^{\mathrm{PP}}, A_2^{\mathrm{PP}}\right)}{\max\left(A_1^{\mathrm{P}}, A_2^{\mathrm{P}}\right)}$$

and

$$A_2^{\mathrm{PP/P}} = \frac{\max\left(A_1^{\mathrm{PP}}, A_2^{\mathrm{PP}}\right)}{\min\left(A_1^{\mathrm{P}}, A_2^{\mathrm{P}}\right)}, \tag{4}$$

[1]Seismological Laboratory, California Institute of Technology, Pasadena, USA.
[2]Institut de Physique du Globe, Université Louis Pasteur, Strasbourg, France.
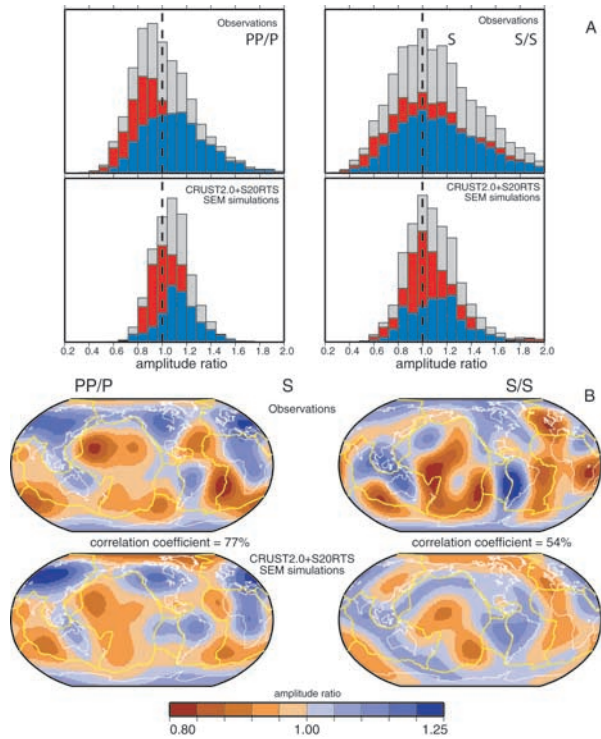[3]Now at Shell International Exploration and Production, Rijswijk, The Netherlands.

**Figure 1.** (a) Histograms of PP/P (left) and SS/S (right). The data are grouped according to whether the associated PP (or SS) surface reflection point is underneath the oceans (red) or continents (blue). (b) PP/P (left) and SS/S (right) amplitude ratios with respect to PREM and Harvard CMT source parameters, plotted at the PP surface reflection point. The top panel shows the observed amplitude ratios, while the lower panel shows amplitude ratios determined from the SEM synthetics. The large-scale trends in PP/P and SS/S are emphasized by expanding their values in spherical harmonics up to degree and order 6. The correlations between the observed and SEM predicted PP/P and SS/S maps are, respectively, 77% and 54%.

which are minimum and maximum estimates of the PP/P amplitude ratio, respectively. The best estimate of PP/P and its uncertainty is

$$PP/P = \frac{A_1^{pp/p} + A_2^{pp/p}}{2} \pm \frac{A_2^{pp/p} - A_1^{pp/p}}{2}. \qquad (5)$$

We retain measurements of PP/P when

$$\frac{\left| A_2^{pp/p} - A_1^{pp/p} \right|}{A_1^{pp/p} + A_2^{pp/p}} < 0.1. \qquad (6)$$

This corresponds to data with a least-squares waveform fit between $d(t)$ and $s(t - \tau_m)$ in the P and PP windows, i.e., after the time shift $\tau_m$ has been applied, of at least 80%. Our data set includes 10,550 PP/P measurements at epicentral distances larger than 55°. We apply the same measurement procedure and selection criteria to transverse component waveform data to obtain 7,250 SS/S amplitude ratio measurements.

### 2.2. 3-D Model Simulations

[6] We simulate PP/P and SS/S amplitude ratios by applying equations (5) and (6) to synthetic vertical and transverse component seismograms, respectively. These synthetics are computed using the Spectral-Element Method (SEM) [*Komatitsch and*

*Tromp*, 2002a, 2002b] for crustal model CRUST2.0 [*Bassin et al.*, 2000], model ETOPO5 of ocean bathymetry and topography [*NOAA*, 1988], and 3-D models of S and P wave velocity heterogeneity in the mantle. Model S20RTS [*Ritsema et al.*, 1999] is used to describe S velocity variations in the mantle. The P velocity heterogeneity in the mantle is assumed to be identical to that of S20RTS, except for a depth-dependent scaling factor R = $dlnV_s/dlnV_p$, which increases linearly from 1.3 at the surface to 3.0 at the core-mantle boundary [*Ritsema and van Heijst*, 2002]. The structure is identical to that in PREM.

[7] Since the SEM simulations are time consuming (~40 hours per simulation on a PC cluster with 151 733 MHz CPUs), we limit ourselves to calculating synthetic seismograms for 50 worldwide earthquakes at about 400 global and regional network stations. The number of synthetic seismograms is similar to the number of recordings, ensuring that the gross characteristics of the data are simulated accurately.

## 3. Global Distribution of PP/P

[8] The global distribution of PP/P amplitude ratios has a strong ocean/continent correlation (Figure 1a). PP/P is, on average, ~0.85−0.90 (i.e., the PP amplitude is smaller than predicted by PREM) when PP reflects off oceanic crust while PP/P is evenly distributed about 1 for continental PP reflection points. A relatively high average value of ~1.10−1.15, compared to the PREM predicted value, is obtained for PP/P data with PP reflections points within continents.
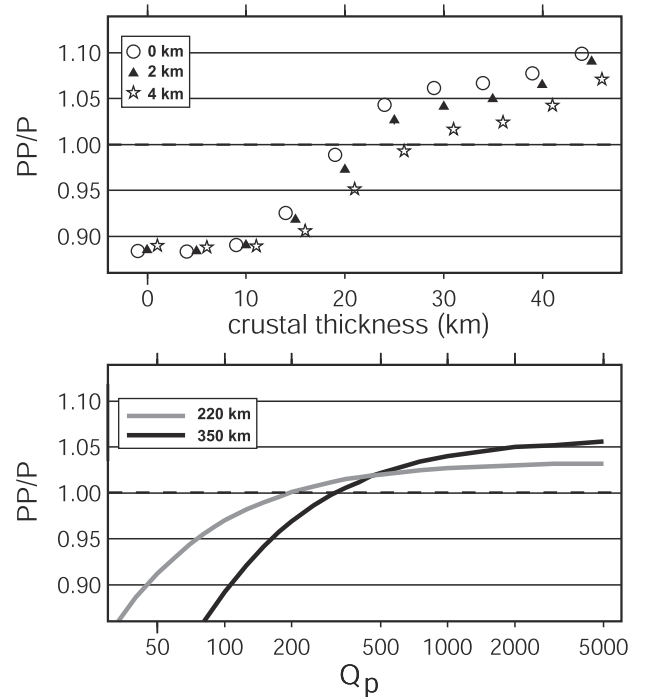


**Figure 2.** (a) Predictions of PP/P amplitude ratios for models with the same seismic velocity, density, and Q structure as in PREM, but in which the thickness of the crust is varied between 0 and 50 km and the ocean has a water depth of 0 km (circle), 2 km (triangle), or 4 km (star). The effect of an ocean on PP/P is large only when the crust is thicker than 15 km. These models are irrelevant since oceanic crust is typically thinner than 10 km. (b) Predictions of PP/P for models in which a constant value of $Q_p$ in the uppermost 220 km (light grey line), or uppermost 350 km (dark grey line) of the mantle is varied. The velocity and density structures are the same as in PREM.
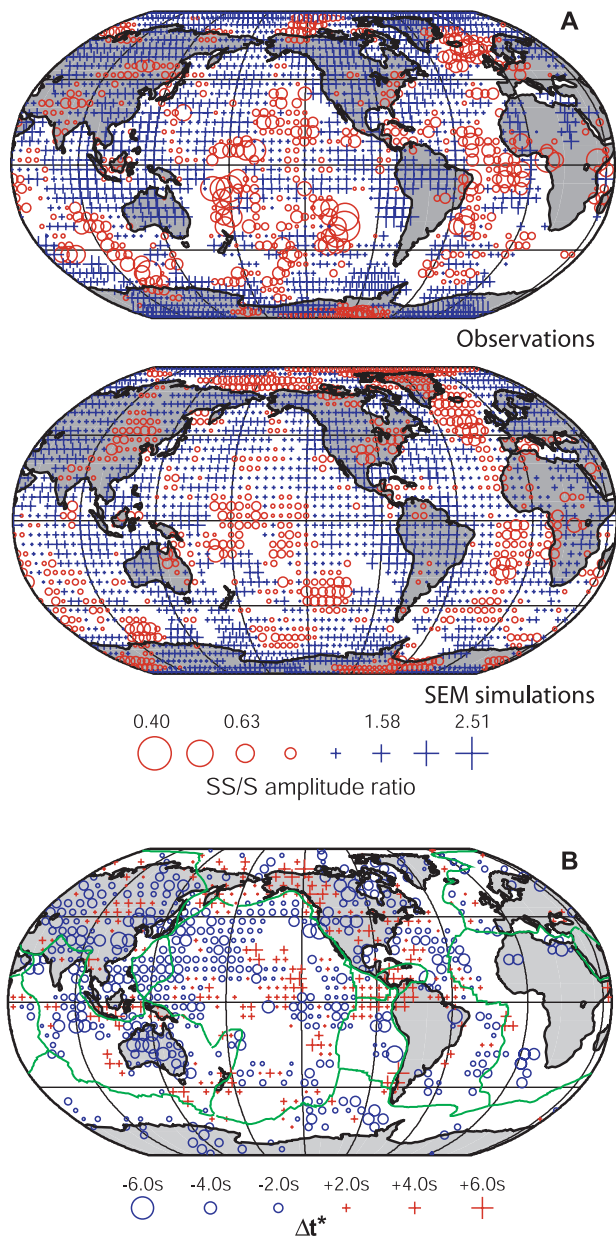
**Figure 3.** (a) Observed (top) and SEM predicted (bottom) SS/S amplitude ratios with respect to PREM and Harvard CMT source parameters plotted at SS surface reflection points. Red circles represent negative SS/S residuals with respect to PREM, while blue '+' symbols represent positive SS/S anomalies. (b) $\Delta t^{\star}_{SS-S}$ distribution from *Reid et al.* [2001]. SS waveforms associated with positive (negative) $\Delta t^{\star}_{SS-S}$ values are relatively broad (narrow) compared to SS waveforms simulated using the PREM model. The data in both (a) and (b) have been smoothed by averaging at least 3 residuals with SS reflection points that fall within a circular cap with a radius of $5°$. It is expected that negative (positive) SS/S residuals correlate with positive (negative) values of $\Delta t^{\star}_{SS-S}$.

[9] The ocean/continent distribution of PP/P is sensitive to crustal thickness variations. Figure 2 shows that values of PP/P between 0.9 (oceans) and 1.15 (cratons) can be explained by the effect of crustal thickness on the long-period PP reflection coefficient. The PP reflection coefficient relative to the reflection coefficient for PREM, in which the crust is 21.4 km thick, varies from 0.9 to 1.1 when the crust ranges in thickness from 0 to 45 km, in agreement with the observed range of PP/P values. The ocean/

continent variation of PP/P is well reproduced by predictions from SEM synthetics (Figure 1b), which incorporate CRUST2.0 crustal thickness variations.

[10] Alternatively, a low value of $Q_p$ in the upper mantle can also explain the relatively low PP/P amplitude ratios for oceanic PP reflection points. PP/P values of $0.90-0.95$ are predicted when $Q_p$ in the uppermost 220 km of the mantle is as low as $50-75$. However, high PP/P amplitude ratios cannot be explained by relatively high $Q_p$ values in the upper mantle because even in PREM long-period PP attenuates little. We therefore attribute most of the observed PP/P variation to the variable thickness of the crust.

## 4. Global Distribution of SS/S

[11] The predictable effect of crustal thickness on PP/P ratios demonstrates that the large-scale variation of PP/P can be determined accurately. Since SS/S is measured in the same manner and with similar accuracy as PP/P, the large-scale, but complex, variation seen in SS/S is robust.

[12] SS/S amplitude ratios do not clearly correlate with surface geology. The high geometric mean value of $1.09 \pm 0.05$ of SS/S measurements (Figure 1a) and their large-scale geographic variation (Figure 1b) are similar to the SEM predicted geometric mean value ($1.07 \pm 0.02$) and the SEM predicted geographic variation. Maps of the observed and SEM-predicted SS/S, expanded in spherical harmonics up to degree and order 6, both show minima of SS/S in the central and southern Pacific and northwestern Europe and a maximum beneath South America. The correlation coefficient between these maps is 54%.

[13] The geographic variation of SS/S is similar to the variation of $\Delta t^{\star}_{SS-S}$ measurements presented by *Reid et al.* [2001] (Figure 3), especially in eastern Asia and the Pacific, where overlapping coverage is best. $\Delta t^{\star}_{SS-S}$ quantifies SS waveform broadening. It is expected that high values of SS/S correlate with low values of $\Delta t^{\star}_{SS-S}$ and, vice versa. The good correlation further underscores that SS/S and $\Delta t^{\star}_{SS-S}$ are meaningful data, albeit that, in disagreement with *Reid et al.* [2001], we prefer not to attribute the data patterns entirely to attenuation.

## 5. Conclusions

[14] While differential body-wave traveltimes have often been used to constrain seismic velocity variations in the mantle [e.g., *Woodward and Masters*, 1991; *Kuo et al.*, 2000], we have demonstrated that coherent patterns of PP/P and SS/S amplitude ratios can also be determined from a large set of high-quality digital waveform data.

[15] Measurements of PP/P and SS/S using SEM seismograms that incorporate the effects of wave propagation through a 3-D crust and mantle model reproduce the gross characteristics of the data. The PP/P amplitude ratio appears to be determined mostly by the reflection coefficient of PP and yields a clear ocean/continent variation. Like surface-wave amplitudes, SS/S amplitude variations point to the significant effects of velocity gradients in the mantle on wave propagation.

[16] SS/S data are valuable for refining shear-velocity models of the mantle. Moreover, constraining attenuation in the (deep) mantle using body-wave amplitudes must go hand-in-hand with analysis of the effects of focusing and defocusing on body-wave amplitudes.

## References

Bassin, C., G. Laske, and G. Masters, The current limits of resolution for surface wave tomography in North America, *Eos Trans. AGU*, F897, 2000.

Bhattacharyya, J., G. Masters, and P. Shearer, Global lateral variations of shear wave attenuation in the upper mantle, *J. Geophys. Res.*, *101*, 22,273–22,289, 1996.

Billien, M., J.-J. Lévêque, and J. Trampert, Global maps of Rayleigh wave attenuation for periods between 40 and 150 s, *Geophys. Res. Lett.*, *27*, 3619–3622, 2000.

Durek, J. J., M. H. Ritzwoller, and J. H. Woodhouse, Constraining upper mantle anelasticity using surface wave amplitudes, *Geophys. J. Int.*, *114*, 249–272, 1993.

Dziewonski, A. M., Global seismic tomography: past, present, and future, in *Problems in Geophysics for the New Millennium*, edited by E. Boschi, G. Ekström, and A. Morelli, pp. 289–350, Istituto Nazionale di Geofisica e Vulcanologia, Roma, 2000.

Dziewonski, A. M., and D. L. Anderson, Preliminary Reference Earth Model, *Phys. Earth Planet. Inter.*, *25*, 297–356, 1981.

Komatitsch, D., and J. Tromp, Spectral-element simulations of global seismic wave propagation – I. Validation, *Geophys. J. Int.*, in press, 2002a.

Komatitsch, D., and J. Tromp, Spectral-element simulations of global seismic wave propagation – II. 3-D models, oceans, rotation, and self-gravitation, *Geophys. J. Int.*, in press, 2002b.

Kuo, B.-Y, E. J. Garnero, and T. Lay, Tomographic inversion of S-SKS times for shear velocity heterogeneity in D″: Degree 12 and hybrid model, *J. Geophys. Res.*, *105*, 28,139–28,158, 2000.

NOAA, National Oceanic and Atmospheric Administration product information catalog – ETOPO5 Earth Topography 5-minute digital model, *Tech. Rep.*, U.S. Department of Commerce, Washington, D.C., 171 pp., 1988.

Reid, F. J. L., J. H. Woodhouse, and H. J. van Heijst, Upper mantle attenuation and velocity structure from measurements of differential S phases, *Geophys. J. Int.*, *145*, 615–630, 2001.

Ritsema, J., and H. J. van Heijst, Constraints on the correlation of P-wave and S-wave velocity heterogeneity in the mantle from P, PP, PPP, and PKPab travel-times, *Geophys. J. Int.*, in press, 2002.

Ritsema, J., H. J. van Heijst, and J. H. Woodhouse, Complex shear velocity structure imaged beneath Africa and Iceland, *Science*, *286*, 1925–1928, 1999.

Romanowicz, B., The upper mantle degree 2. Constraints and inferences from global mantle wave attenuation measurements, *J. Geophys. Res.*, *95*, 11,051–11,071, 1990.

Romanowicz, B., A global tomographic model of shear attenuation in the upper mantle, *J. Geophys. Res.*, *100*, 12,375–12,394, 1995.

Selby, N. D., and J. H. Woodhouse, Controls on Rayleigh wave amplitudes: attenuation and focusing, *Geophys. J. Int.*, *142*, 933–940, 2000.

Woodhouse, J. H., and Y. K. Wong, Amplitude, phase and path anomalies of mantle waves, *Geophys. J. Int.*, *87*, 753–773, 1986.

Woodward, R. L., and G. Masters, Global upper mantle structure from long-period differential travel times, *J. Geophys. Res.*, *96*, 6351–6377, 1991.

—————————

D. Komatitsch, J. Ritsema, and J. Tromp, Seismological Laboratory 252-21, California Institute of Technology, Pasadena, CA 91125, USA. (jeroen@gps.caltech.edu)

L. A. Rivera, Institut de Physique du Globe, Université Louis Pasteur, 5 Rue René Descartes, F-67084 Strasbourg cedex, France.

H.-J. van Heijst, Shell International Exploration and Production, Postbus 60, Rijswijk, Netherlands.